

1 **LPDynR: a new tool to calculate the Land Productivity**

2 **Dynamics indicator**

3 Xavier Rotllan-Puig¹, Eva Ivits², and Michael Cherlet³. 

4
5 ¹ ASTER Projects. Barri Reboll, 9, 1r. 08694 Guardiola de Berguedà (Barcelona), SPAIN

6 ² European Environment Agency. Geospatial Information Services Group. Copenhagen,
7 DENMARK

8 ³ European Commission – Joint Research Centre (JRC). Directorate D – Sustainable
9 Resources. Unit D6 – Knowledge for Sustainable Development & Food Security Unit.
10 Via Enrico Fermi 2749. I-21027 Ispra (VA), ITALY

11  Correspondence: Michael Cherlet <michael.cherlet@ec.europa.eu>

12
13
14
15 **Keywords:** Land Productivity, Ecosystem Dynamics, Land Degradation, Desertification,
16 Vegetation

17

18 **Abstract**

19 As part of the UN Sustainable Development Goal 15 (Life on Land), the indicator 15.3.1
20 is adopted to measure the Land Degradation Neutrality. Land Degradation Neutrality is
21 addressed as stable —or increasing— state in the amount and quality of land resources
22 required to support ecosystem functions and services and enhance food security during a
23 certain period of time. It is a binary indicator (i.e. degraded/not degraded), expressed as
24 the proportion of land that is degraded over total land area within each land type, and is
25 based on three sub-indicators: (1) Trends in Land Cover, (2) Land Productivity and (3)
26 Carbon Stocks.

27 The Land Productivity sub-indicator (LP) refers to the total above-ground Net Primary
28 Production and reflects changes in health and productive capacity of the land. Declining
29 trends interpreted with ancillary data such as e.g. information on non-adapted agricultural
30 practices possibly combined with low income can be usually understood as land
31 degradation. LP can be calculated using the Land Productivity Dynamics (LPD)
32 approach, which is the methodological basis of the R-based tool *LPDynR* presented in
33 this article. It uses vegetation-related indices (phenology and productivity) derived from
34 time series of remote sensed vegetation indices to estimate ecosystem dynamics and
35 change. The final result of the LPD indicator is a categorical map with 5 classes of land
36 productivity dynamics, ranging from declining to increasing productivity. As an example
37 of *LPDynR* functionalities, we present a case study for Europe.

38

39 **1 Introduction**

40 The United Nations General Assembly designed in 2015 a collection of 17 global goals,
41 so called Sustainable Development Goals (SDGs; UN, 2015), with the general aim of
42 “achieving a better and more sustainable future for all”, and which are intended to be
43 accomplished by 2030. Each SDG is subdivided into a list of targets which, in turn, go
44 together with indicators to be able to measure their progress and success. Such indicators
45 have to be credible, based on standardized methodologies and, often, have to be spatially
46 explicit (Dubovyk, 2017).

47 The SDG-15, entitled Life on Land, has among its targets the 15.3, which expects “to
48 combat desertification, restore degraded land and soil, including land affected by
49 desertification, drought and floods, and strive to achieve a land degradation-neutral
50 world”. In this context, Land Degradation Neutrality (LDN) is defined as the stable (or
51 increasing) state regarding the amount and quality of land resources required to support
52 ecosystem functions and services and enhance food security during a certain period of
53 time (UNCCD, 2015).

54 The indicator 15.3.1 is adopted to measure the LDN and is expressed as the proportion of
55 land that is degraded over total land area. It is a binary indicator (i.e. degraded/not
56 degraded) based on three sub-indicators calculated separately: (1) Trends in Land Cover,
57 (2) Land Productivity and (3) Carbon Stocks (Sims et al., 2020, 2017). While the first
58 two can capture relatively fast changes, carbon stocks reflect slower changes which
59 suggest a longer-term trajectory (Orr et al., 2017). Following a “one-out-all-out” process,
60 the indicator identifies an area as degraded if one of the sub-indicators shows

61 degradation. The three sub-indicators must be comparable among territories and based on
62 standardized sources and methods. The data can be collected through existing sources,
63 such as maps, reports or databases, but also can be derived from Earth observation (EO)
64 imagery using remote sensing tools.

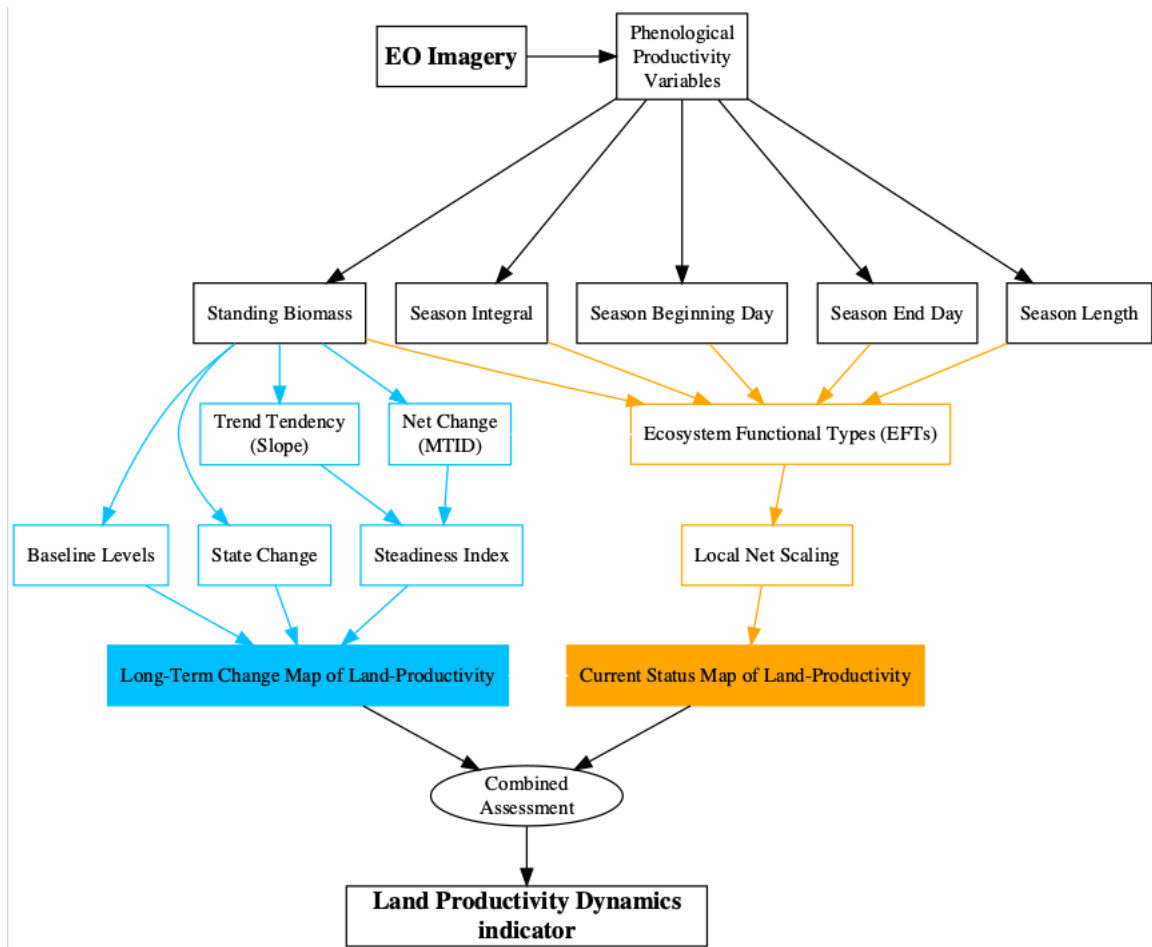
65 The Land Productivity sub-indicator (LP), addressed in this document, approximates the
66 total above-ground net primary productivity (NPP), which can be defined as the total
67 energy fixed by plants minus their respiration. Such energy is transformed into biomass
68 which, in turn, allows ecosystems to develop their functions and deliver essential
69 services. Therefore, LP reflects changes in health and productive capacity of the land and
70 its declining trends can be usually understood as land degradation (Cherlet et al., 2018;
71 Prince, 2009; Yengoh et al., 2015). The World Atlas of Desertification (Cherlet et al.,
72 2018) suggests that the LP sub-indicator can be calculated using the Land Productivity
73 Dynamics (LPD) approach. LPD was first developed by Ivits and Cherlet (2013) and is
74 the methodological basis of the *LPDynR* tool presented in this article.

75 **2 Land Productivity Dynamics and *LPDynR***

76 The Land Productivity Dynamics (LPD) approach is based fundamentally on the use of
77 time series of vegetation-related indices derived from remote sensed imagery, such as the
78 normalized difference vegetation index (NDVI) or the plant phenology index (PPI).
79 NDVI, for example, can be used as a proxy for land productivity, as many studies at
80 global and local scales have identified a strong relationship between NDVI and NPP
81 (Ivits and Cherlet, 2013; Prince, 2009; Yengoh et al., 2015, and references therein). The
82 LPD approach often uses phenological and productivity-related variables derived from

83 time series of NDVI, given that these can provide additional information on several
84 aspects of vegetation/land cover functional composition in relation to ecosystem
85 dynamics and change (E. Ivits, M. Cherlet, Mehl, et al., 2013). These dynamics of the
86 ecosystems, which might eventually drive land degradation, can be caused by human
87 activities and/or biophysical processes, as well as other processes indirectly tied to them,
88 such as climate change (Yengoh et al., 2015). While the most commonly used
89 phenological parameters are the beginning and the end date of the vegetation growing
90 season, together with the season length in number of days, the ones related to land
91 productivity are e.g. accumulations of vegetation index values over time, mostly during
92 the growing season as defined by the season start and end date. These approximate NPP
93 within the growing season.

94 The final result of the LPD indicator is a categorical map with 5 classes of land
95 productivity dynamics, ranging from declining to increasing productivity over a target
96 time period. It is the result of a combined assessment of two sources of information, as
97 seen in Figure 1. The first layer is the Long-Term Change Map. In general terms, it
98 shows the tendency of change of land productivity (positive or negative) and the effect on
99 productivity levels that this tendency might have had on a particular original point after a
100 certain period of time. The second layer is the Current Status Map, which provides
101 information on the current levels of land productivity in relation to its potential, being
102 current the end of the target time period. It compares the local productivity with the range
103 of productivity across similar areas in terms of land cover or bioclimatic traits (Sims et
104 al., 2017). Further explanations for both branches will be given in the respective sections
105 below.



106

107 *Figure 1: Flowchart of the process to calculate the Land Productivity Dynamics indicator and*
108 *used by LPDynR*

109

110 Following the LPD approach, *LPDynR* is an R-based tool (i.e. an R package) which
111 allows the user to produce the final Land Productivity Dynamics Map using as inputs a
112 set of time series of phenological and/or productivity variables (multi-band GeoTIFF
113 rasters). By means of the different functions included in the package, it produces
114 intermediate layers (e.g. Steadiness Index, Ecosystem Functional Types; see Figure 1)
115 which are used to calculate both the Long-Term Change Map and the Current Status

116 Map. In addition, several parameters can be set along the process in order to reflect the
117 preferences of the user. The functions included in the package have no limitations
118 regarding the number of years included in the time series, the variables to use or the
119 spatial extent and resolution. While *LPDynR* v1.0.1 can be installed from CRAN
120 (<https://CRAN.R-project.org/package=LPDynR>), the latest version is available at
121 <https://github.com/xavi-rp/LPDynR>.

122 **3 Data set preparation**

123 A case study is presented in order to illustrate the methodology implemented in the
124 *LPDynR* package to calculate the LPD indicator. In this case, a data set of 5 phenological
125 and productivity-related variables were used, at European level and on a 0.5km of spatial
126 resolution, produced by the European Environment Agency - European Commission
127 (EEA). They are all derived from time series (2000-2019) of MODIS imagery and its
128 derived product Plant Phenology Index (PPI; Jin and Eklundh, 2014). PPI is linearly
129 related to the canopy green leaf area index (LAI) and has a temporal pattern very similar
130 to the one shown by the gross primary productivity (GPP) estimated by flux towers at
131 ground reference stations. The five variables are produced using the software TIMESAT
132 (Jönsson and Eklundh, 2004). At the moment of writing this article, these time series are
133 not yet published, however more information about the previous freely distributed data
134 set (2000-2016) by the EEA can be found in their website
135 (<https://sdi.eea.europa.eu/catalogue/srv/eng/catalog.search#/home>). For example, the
136 details for above ground vegetation productivity can be found in

137 <https://sdi.eea.europa.eu/catalogue/srv/eng/catalog.search#/metadata/29ae2d47-7af2->

138 [4c09-ba5f-e2fbb7c2b0d1](https://sdi.eea.europa.eu/catalogue/srv/eng/catalog.search#/metadata/29ae2d47-7af2-4c09-ba5f-e2fbb7c2b0d1). The five variables used were:

- 139 • Above ground vegetation productivity (from now on, SB)
- 140 • Above ground season vegetation productivity (from now on, CF)
- 141 • Start of vegetation growing season (from now on, SBD)
- 142 • End of vegetation growing season (from now on, SED)
- 143 • Vegetation growing season length (from now on, SL)

144 In the *LPDynR* v.1.0.1, the functions use multi-band GeoTIFF rasters to start the process,
145 one per phenological/productivity variable. Each band of each raster contains one of the
146 years of the time series.

147 It is also important to note that *LPDynR* comes with a sample data set, which can be used
148 to run tests, as well as some examples in the form of “vignettes” attached to the package.

149 **4 Long Term Change Map of land productivity**

150 As seen in Figure 1 and explained above, the Land Productivity Dynamics indicator is
151 produced by combining two input layers. The first layer is the Long-Term Change Map
152 (also called “tendency map”). The tendency layer combines information on the trend of
153 land productivity dynamics (positive or negative), the level of productivity of the
154 ecosystem at the start of the time series, as well as whether it has changed its productivity
155 state or not in the period under study (Ivits and Cherlet, 2013). Using such multi-source
156 information for the Long-Term Change Map instead of a trend significance assessment

157 was chosen to better describe the state and change of ecosystems. For instance, even
158 though vegetation development presents a long-term negative dynamics (e.g. negative
159 slope of a linear trend), the negative trend might not be strong enough to decrease the
160 level of productivity such that the starting productivity state changes drastically. This
161 could result to be a non-significant trend in linear trend analysis leaving the pixel out for
162 further analysis which is not wishful in the land degradation analysis. The way in which
163 the three sources of information are calculated for the Long Term Change Map using a
164 land productivity variable is described in the following subsections.

165 **4.1 Steadiness Index**

166 The first of the three metrics which integrates the Long-Term Change Map represents the
167 long-term tendency of change of the natural systems, being either positive or negative.
168 This metrics is the Steadiness Index (Ivits, Cherlet, Sommer, et al., 2013) and can be
169 calculated using the function *steadiness()*. The Steadiness Index is based on the
170 combination of two other metrics which are calculated per pixel by the same function: (1)
171 the slope derived from fitting a linear trend on the time series and (2) the net change of
172 the productivity level of the same period.

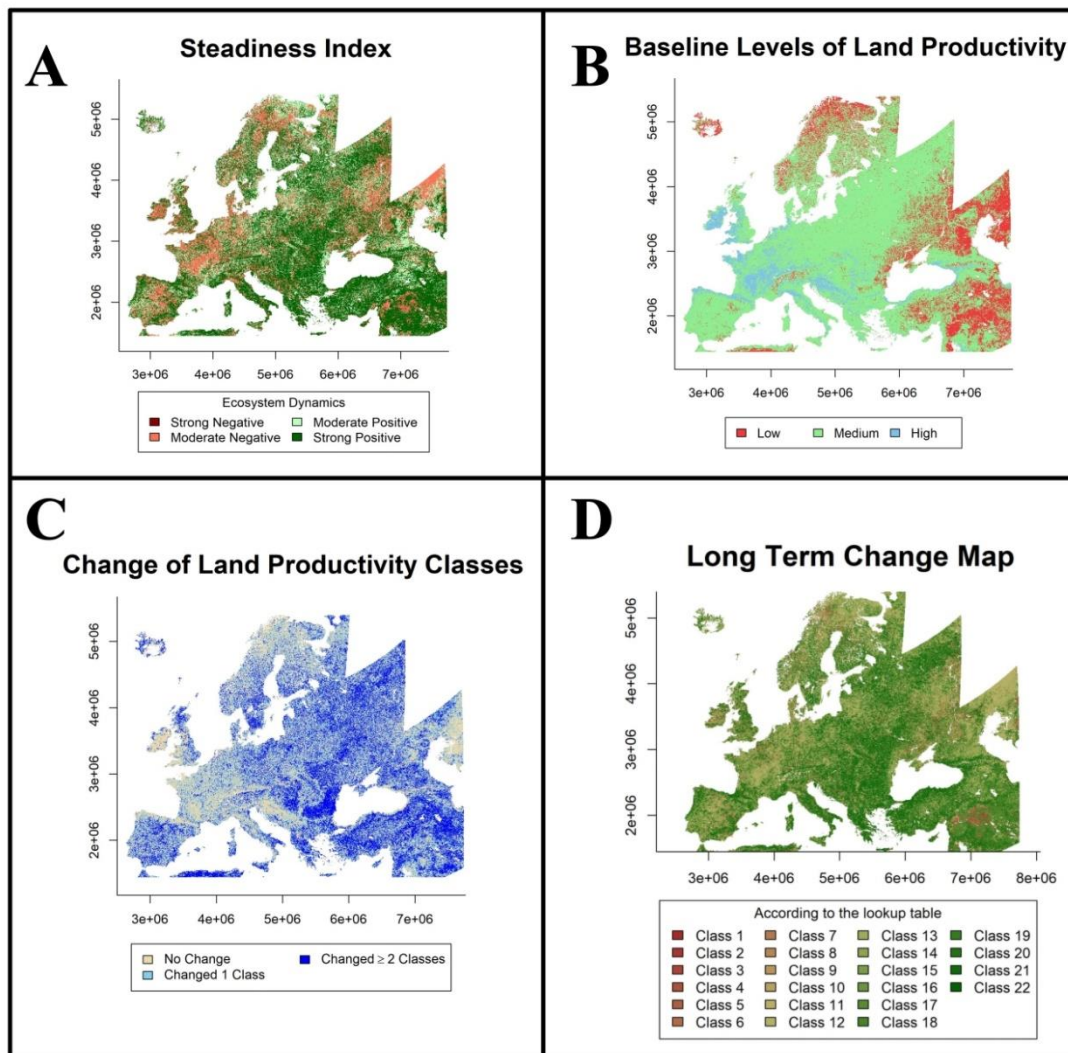
173 The use of a linear regression would imply to respect the linear trend results by strict
174 statistical assumptions for confidence intervals and significance tests, such as
175 heteroscedasticity, normal distribution of the errors, no autocorrelation between the
176 observations and a deterministic process. Most often, these assumptions are not
177 accomplished when working with time series of remote sensed products, and the use of
178 non-parametric trend measures are not adequate either (Ivits, Cherlet, Sommer, et al.,

179 2013). This is why the Steadiness Index only keeps classes of tendency and no more tests
180 are run for assessing its significance. Therefore, only the sign (positive or negative) of the
181 slope of the trend is kept as the value of each pixel’s tendency of ecosystem dynamics. In
182 addition, the net change of the productivity variable, in the units of the applied vegetation
183 index, is calculated for the same time window and per pixel using the Multi-Temporal
184 Image Differencing method (MTID; Guo et al., 2008). Afterwards, MTID is also
185 transformed into positive or negative net change. Finally, the two classes of both metrics
186 (slope of the linear function and net change category) are combined into four “steadiness”
187 categories as seen in Table 1. Figure 2A represents the 4-class map of the Steadiness
188 Index for the case study.

189 *Table 1: Description of the four Steadiness Index classes and how they are derived based on the*
190 *combination of the signs of both the slope of the linear function and the net change*

Steadiness Class	Slope	Net Change	Description
Steadiness1	-	-	Strong negative ecosystem dynamics (possibility changing equilibrium)
Steadiness2	-	+	Moderate negative ecosystem dynamics (likely remain in current equilibrium)
Steadiness3	+	-	Moderate positive ecosystem dynamics (likely remain in current equilibrium)
Steadiness4	+	+	Strong positive ecosystem dynamics (possibility changing equilibrium)

191



192

193 *Figure 2: (A) Steadiness Index, (B) baseline levels and (C) state change maps for the case study*
 194 *based on the 'Above ground vegetation productivity' variable. (D) Land productivity Long Term*
 195 *Change Map for the case study based on the combination of the previous three maps.*

196

Descriptions respectively in sections 4.1, 4.2, 4.3 and 4.4

197

198 **4.2 Baseline levels of productivity**

199 The second source of information for the derivation of the Long-Term Change Map is the
200 baseline levels of the productivity variable at the beginning of the time series.

201 For the calculation of the baseline levels of land productivity at the beginning of the time
202 series, *LPD_{ynR}* categorizes productivity values into three classes: low, medium and high.

203 To do that, the function *baseline_lev()* averages the first *n* years of the time series in
204 order to avoid extreme events, such as abnormal droughts in wet areas, etc, which would
205 skew the distribution of productivity values into too high or low values. The number of
206 years to be considered by the average function can be set by passing the argument
207 *yearsBaseline* to the function. The default value is 3 years; averaging more years would
208 move the baseline value closer to the mean of the time series, which would not describe
209 the baseline anymore.

210 After the average of the *n* number of years is calculated, *baseline_lev()* first classifies the
211 pixels into 10 classes using 10-quantiles equalling to the corresponding percentile levels.

212 The reason for this intermediate step is that, if directly opted for three classes (i.e. low,
213 medium and high), the number of pixels per category would be classified homogeneously
214 (i.e. 33.3% of pixels/class), which is a statistically correct but an over simplified
215 representation of baseline status. Instead, *LPD_{ynR}* allows the user to define the percentile
216 level to be used based on local knowledge. For example in dryland ecosystems or in
217 boreal regions different average productivity level can be defined as low, medium or high
218 values. The United Nations Development Programme (UNPD, <https://www.undp.org>) for
219 example declares that 40% of the World's land resources are drylands (Middleton et al.,

220 2011), while the World Atlas of Desertification updated this proportion to 37.2% (Cherlet
221 et al., 2018). Therefore, in global applications one might choose 37.2% of pixels to be
222 classified as “low level” of productivity. Consequently, as default, the global application
223 of *LPDynR* classifies the first four groups of pixels, i.e. 40 percentile (after rounding
224 37.2%), as “low” baseline productivity level, the five consecutive groups between 50 and
225 90 percentile as “medium” productivity level and the rest 10% of pixels with the highest
226 average productivity levels, as “high” baseline. Both the proportion of pixels classified as
227 low level and high level of land productivity can be set by passing to *baseline_lev()* the
228 arguments *drylandProp* and *highprodProp*, respectively. The function classifies the rest
229 of the pixels $((100 - (drylandProp + highprodProp)))$ as medium level. The assumption of
230 classifying 40% of pixels as low productive is valid at global level, however, the
231 proportion of drylands/low level of productivity should be modified for local and regional
232 studies. For example, at the European level, drylands cover 20% of total land (FAO,
233 2019). This proportion has been used in the case study and the resulting 3-class map
234 showing the estimation of levels of productivity at the beginning of the time series can be
235 seen in Figure 2B.

236 **4.3 Change of state of productivity**

237 The third layer used for the land productivity Long-Term Change Map is the change of
238 the state of the productivity level during the time window under study. This aspect is
239 necessary for land degradation assessments as it reports whether pre-set productivity state
240 thresholds have been surpassed or not, which can be a consequence of either the natural

241 resilience, new land use/practices that have been introduced, or impacts of other
242 manmade or natural phenomena (Ivits and Cherlet, 2013).

243 To calculate the state change per pixel, the function *state_change()* uses both the
244 productivity baseline level at the beginning of the time series, as described in the
245 previous subsection, and the productivity state level at the end of the time series. This
246 final state is calculated in the same way as the baseline level, i.e. (1) averaging the last 3
247 years and (2) classifying into 10 categories using 10-quantiles. The reason for using a 10-
248 class classification is that it would be difficult to approximate if the change of one state to
249 another was due to a big or a small change. Instead, using the 10-class classification for
250 the final productivity state, one can address if a pixel has moved from class 5 to 4 (small
251 change) or from class 9 to 4 (big change).

252 Once the class change per pixel has been calculated, either with positive or negative
253 results, the map is categorized into 3 final classes: (1) no change, (2) changed between 1
254 and x classes or (3) changed more than x classes, where x can be defined by the user by
255 passing the argument *changeNclass* to the function (default is 1). See Figure 2C for a
256 map of the state change in the case study.

257 **4.4 Long Term Change Map**

258 The land productivity Long-Term Change Map is one of the two pillars of the LPD
259 indicator (Figure 1) calculated with *LPDynR*. This map is calculated by the combination
260 of the Steadiness Index, the productivity levels at the beginning of the time series and the
261 change of the state of productivity between the beginning and the end of the time series.

262 The function *LongTermChange()* performs the combination of the three qualitative
 263 metrics mentioned before into the Long-Term Change Map, resulting in 22 new
 264 categories as shown in Table 2. The resulting map for the case study is presented in
 265 Figure 2D.

266

267 *Table 2: Lookup table for the land productivity Long Term Change Map (Steadiness Index +*
 268 *BaseLine Levels + State Change)*

	Change of productivity at the end of the time series		
	No Change	Changed 1 to x classes	Changed $> x$ classes
Steadiness Index / Baseline productivity			
St1 low	1	2	3
St1 med.	4	5	6
St1 high	7	8	9
St2 low	10	10	10
St2 med.	11	11	11
St2 high	12	12	12
St3 low	13	13	13
St3 med.	14	14	14
St3 high	15	15	15
St4 low	16	17	18
St4 med.	19	20	21
St4 high	22	22	22

269

270 At this point, the user might want to finalise the LPD calculation avoiding the second part
 271 of the methodology proposed by Ivits and Cherlet (2013), which is the Current Status
 272 Map of Land Productivity. To do this, the function *LPD_CombAssess* (see further

273 explanations in the respective subsection below) can be called to reclassify the 22-class
274 Long-Term Change Map into the final 5 classes of LPD.

275 **5 Current Status Map of land productivity**

276 The Land Productivity Dynamics indicator is composed of two base layers: the Long-
277 Term Change Map of Land Productivity and the Current Status Map of Land Productivity
278 (as shown in Figure 1). After the long-term productivity dynamics described previously
279 (i.e. Long-Term Change Map) is calculated, the second source of information needed is
280 the current level of land productivity. For this purpose, a Local Net Scaling approach is
281 implemented (Prince, 2009). Such approach estimates the level of land productivity of
282 each pixel relative to its neighbours with similar characteristics of their land functions. In
283 other words, it calculates the potential level of productivity of each pixel within a
284 homogeneous land unit. The Current Status Map may help, for instance, to identify areas
285 which, although having a positive trend of productivity over time, their levels of current
286 productivity are low relative to the pixels in the same homogeneous land unit and, thus,
287 they might be still suffering land degradation (Sims et al., 2017). A first step for the
288 calculation of the Current Status Map, therefore, is the derivation of the homogeneous
289 land units across the area of study.

290 **5.1 Ecosystem Functional Types (EFTs)**

291 The methodology implemented in *LPD_{dynR}* to derive homogeneous land units, or
292 Ecosystem Functional Types (EFTs), is adapted from Ivits, Cherlet, Horion et al. (2013).
293 It is basically a clustering process which uses, in this case, phenological and productivity

294 variables to create the ecosystem functional groups. Among the different unsupervised
295 clustering techniques available for data grouping, K-means has been chosen. K-means is
296 widely used in data science mainly due to its relative simplicity of implementation and
297 interpretation.

298 Originally, the unsupervised classification was performed after a three-steps pre-
299 processing of the phenology and productivity variables (see Chapter 3, Dataset
300 preparation): (1) removing highly correlated variables to avoid multicollinearity; (2) a
301 first Principal Component Analysis (PCA) to select the optimal number of PCs and their
302 associated variables showing the highest loadings; and (3) a final PCA to clearly
303 associate each PC with one variable. However, test runs in this study (see Supplementary
304 Material S1) have shown that the final LPD indicator does not differ significantly when it
305 is derived using the raw phenological/productivity variables. Therefore, although the two-
306 PCAs step is also implemented in *LPD_{dynR}*, only the removing of highly correlated
307 variables (e.g. $|r| > 0.7$) is recommended before running the k-means clustering.

308 In order to check for multicollinearity among the variables, the function *rm_multicol()*
309 first calculates their averages among the years of the time series. Then, the process
310 internally runs the function *removeCollinearity()* from the package *virtualspecies* (Leroy
311 et al., 2016). This function allows the user to set up the minimum Pearson's correlation
312 absolute value, which can be modified by passing the argument *multicol_cutoff*. It is
313 established to be $r = 0.7$ as default. A subset of random points of the data set can be used
314 for the calculation of the correlation coefficient in case the rasters have a large number of
315 pixels and the user wants to speed up the process. The default number of randomly
316 selected points is 10% of total pixels in the raster. However, the number of points can be

317 selected by passing *sample.points = FALSE* and *nb.points* equal to the required amount
318 of points. Finally, the function automatically creates a multi band raster where each band
319 corresponds to one randomly selected variable of each group of correlation. In addition, a
320 dendrogram to visualize the groups of intercorrelated variables can be plotted if the user
321 wants to, although not by default. For the present case study, which was run with five
322 variables, the dendrogram produced can be seen in Supplementary Material S2. At the
323 cut-off value of $r = 0.7$, three groups of intercorrelated variables were found and one
324 variable of each group was selected to continue with the analysis (i.e. CF, SED and SL).

325 In case the user would like to run the two-PCAs steps, both the first “screening PCA”,
326 which is done over the uncorrelated variables, and the “final PCA” are subsequently
327 performed with the same function *PCAs4clust()*. In order to know the optimal number of
328 variables to be used in the “final PCA”, a threshold of cumulative variance of the PCs is
329 implemented. This threshold is established to be 0.9, i.e. 90% of the variance of the
330 variables explained, as default.

331 Finally, the clustering algorithm can be run over either the selected PCs or the
332 uncorrelated raw (phenology and productivity) variables using the function *EFT_clust()*.
333 This function uses *kmeans()* from the package *stats*. K-means is an iterative unsupervised
334 method, one of the main limitations being that it is not able to optimize the number of
335 clusters by itself. Instead, the optimal number of clusters needs to be determined by the
336 user. In the *LPDynR* package, the optimal number of clusters can be determined using the
337 “scree-plot method”. This method is implemented with the function *clust_optim()* and it
338 is based on running several K-means clustering with different number of clusters each, in
339 order to assess how the quality of the models change with the number of clusters. Then, a

340 plot is produced with the number of clusters in the x-axis and the total within-cluster sum
341 of squares in the y-axis. A break line, the so-called “elbow”, indicates the number of
342 clusters where the quality of the model no longer improves substantially as the number of
343 clusters (model complexity) increases. In the present study the clustering was run with
344 ten different number of clusters (5 to 50, with the increment of 5) to give a good amount
345 of points to plot the curve, and the maximum number of iterations was set to 10 (see the
346 plot produced in Supplementary Material Figure S3.1).

347 The “scree plot” method undoubtedly has some level of subjectivity, as the user decides
348 where the curve flattens enough for the appropriate number of clusters. Alternatively, to
349 remove such subjectivity, several numerical methods exist to calculate the optimal
350 number of clusters, although they take also some statistical assumptions. These methods
351 might be explored in the future if a higher level of accuracy is believed to be necessary or
352 if the process shall be performed without user intervention. In addition, other hierarchical
353 clustering methods could be explored in order to avoid calculating the optimal number of
354 clusters beforehand, although previous tests run with ISODATA have been shown to be
355 highly resource demanding, especially in terms of computing time.

356 Once the optimal number of clusters is estimated, the final clustering is run with the
357 function *EFT_clust()* using the defined number of clusters and passed with the argument
358 *n_clust*. Other parameters which can be passed to the function *EFT_clust()* are those that
359 will be passed to *stats::kmeans()*, such as *nstart*, *iter.max* or *algorithm* (see
360 <https://stat.ethz.ch/R-manual/R-devel/library/stats/html/kmeans.html> for further
361 information). It is important to note that when setting the argument *nstart*, the larger the
362 value the more accurate the clustering result will be. This is because the function uses

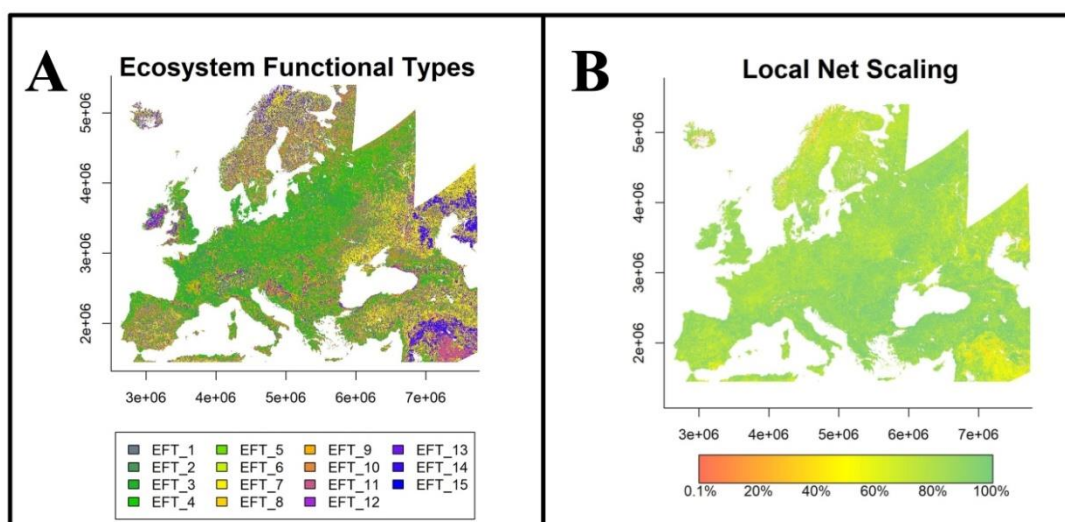
363 different sets of starting random centroids and runs the clustering $nstart$ times. From
364 these number of clustering runs, the best classification result is chosen. Therefore, a
365 larger $nstart$ value increases the chances of having a better cluster classification. In
366 addition, $kmeans()$ can use different algorithms to perform the clustering (e.g.
367 “MacQueen”, “Hartigan-Wong”, etc.; see references in $kmeans()$ documentation). As
368 stated in the function documentation ($?kmeans$), “Hartigan-Wong” usually gives better
369 results, although it is recommended to try several starts ($nstart > 1$). However, when
370 using “Hartigan-Wong” with a (too) large number of clusters, and a lot of values of the
371 variables are very similar, $kmeans()$ is not able to converge in an acceptable amount of
372 time (even increasing the number of iterations with $iter.max$). In these cases when the
373 clustering does not converge, instead of stopping the process with an error, the function
374 $kmeans()$ only gives a warning after finishing the clustering, so that the obtained clusters
375 are based on a non-converged process. Diminishing the number of clusters or rounding
376 variables’ values might be good strategies to help $kmeans()$ to converge.

377 $EFT_clust()$ produces a RasterLayer object, where each pixel is linked to a cluster, plus
378 an index of the clustering performance, which measures the compactness of individuals
379 (i.e. pixels) within the groups. This index, which is expected to be as high as possible, is
380 calculated as:

$$381 \quad CI = \frac{BSS}{TSS} \times 100 \quad (1)$$

382 where CI is the compactness index, BSS is between-cluster sum of squares (i.e.
383 $betweenss$, provided by $kmeans()$) and TSS is total sum of squares (i.e. $totss$, also
384 provided by $kmeans()$).

385 Finally, as previous tests of K-means with up to 100 iterations were showing problems to
386 converge in a certain limit of time, the maximum number of iterations is set to 500 as
387 default in the function. Within this number of iterations and rounding variables, for
388 almost all the tests performed, the process did achieve convergence with no issues (see
389 Supplementary Material S4). For the running example, the EFTs resulted from the whole
390 process can be seen in Figure 3A.



391

392 *Figure 3: (A) Ecosystem Functional Types (EFTs) derived from phenological and productivity*
393 *variables using the K-means clustering method. (B) Local Net Primary Production Scaling*
394 *(LNS): proportion of annual production (i.e. average of the last 5 years of cyclic fraction) over*
395 *the local potential production (i.e. the 90-percentile within the Ecosystem Functional Type)*

396 5.2 Local Net Production Scaling

397 The Local Net Primary Productivity Scaling (from now on, Local Net Scaling or LNS)
398 method (Prince, 2009) is based on the use of multi-temporal satellite data to calculate the
399 difference between the potential and actual NPP for each pixel in homogeneous land

400 functional units. Potential productivity in the *LPDynR* method is defined as the
401 productivity level which could be reached without human influence in natural landscapes
402 (Prince, 2009, and references therein) or as the result of human activity e.g. in agriculture
403 areas or managed forests, and is estimated as the maximum value of productivity within
404 each EFT. The deviation of the productivity found in a particular place and time as
405 referred to the local maximum within its phenological homogeneous cluster, reflects a
406 level of productivity anomaly which is useful for the productivity status map (Ivits and
407 Cherlet, 2013).

408 The cyclic fraction of vegetation productivity (e.g. the summed NDVI over the growing
409 season) is widely used as a proxy for the estimation of the current land productivity
410 (Fensholt, 2013), as it incorporates both natural and anthropogenic factors which define
411 the inter-annual variability of land production. Therefore, it represents that part of the
412 standing biomass which is potentially appropriated to be used by humans and the
413 environment (Ivits and Cherlet, 2013) and it is the one appropriated to calculate the LNS.

414 The function *LNScaling()* is implemented in *LPDynR* to calculate the LNS. The
415 productivity variable (i.e. CF) and the EFTs clusters as explained under 5.1 are passed to
416 *LNScaling()* to calculate the potential productivity within each EFT. Instead of the
417 maximum productivity value within each cluster, the 90-percentile value is established as
418 the potential productivity value, given that values higher than this threshold could be
419 outliers. Finally, the LNS for each pixel is calculated as

420
$$LNS = \frac{AP}{PP_{EFT}} \quad (2)$$

421 where AP is the annual production of the pixel (i.e. the average of the last 5 years of
422 cyclic fraction) and PP_{EFT} is the potential production within its EFT (i.e. the 90-
423 percentile).

424 For the calculation of the final LPD indicator (i.e. combined assessment), the Local Net
425 Scaling values are aggregated into two categories: (1) LNS pixels with less than 50% of
426 the potential local production (within the EFT) and (2) LNS pixels with more or equal to
427 50% of potential local production. This percentage, being 50% the default in LPD_{ynR} ,
428 can be set by the user.

429 The result for the LNS calculation is presented in Figure 3B.

430 **6 Combined assessment of land productivity**

431 The Land Productivity Dynamics indicator, as shown in the processing flowchart in
432 Figure 1, is based on the combination of two main sources of information: a map of the
433 tendency, positive or negative, of the level of land productivity along the time series, and
434 another map capturing the current level of productivity of each pixel relative to the
435 maximum productivity in a homogeneous land area. As seen above, both branches to
436 calculate the indicator are qualitative methods. Therefore, the final LPD indicator,
437 produced with the function $LPD_{CombAssess}()$, is also a qualitative measure with 5
438 possible values or categories after the reclassification of each pixel as shown in Table 3.
439 Such categories are (1) d - Declining, (2) ed - Early signs of decline, (3) st - Stable but
440 stressed, (4) sn - Stable and not stressed and (5) i - Increasing land productivity.

441 *Table 3: Lookup table for the combination of the two branches assessment (i.e. Long Term*
 442 *Change Map and Current Status Map of land productivity) to derive the Land Productivity*
 443 *Dynamics categories (i.e. (1) d - Declining land productivity, (2) ed - Early signs of decline of*
 444 *land productivity, (3) st - Stable but stressed land productivity, (4) sn - Stable and not stressed*
 445 *land productivity and (5) i - Increasing land productivity). The Local Scaling is defined as 50%*
 446 *by default, but it can be modified by the user*

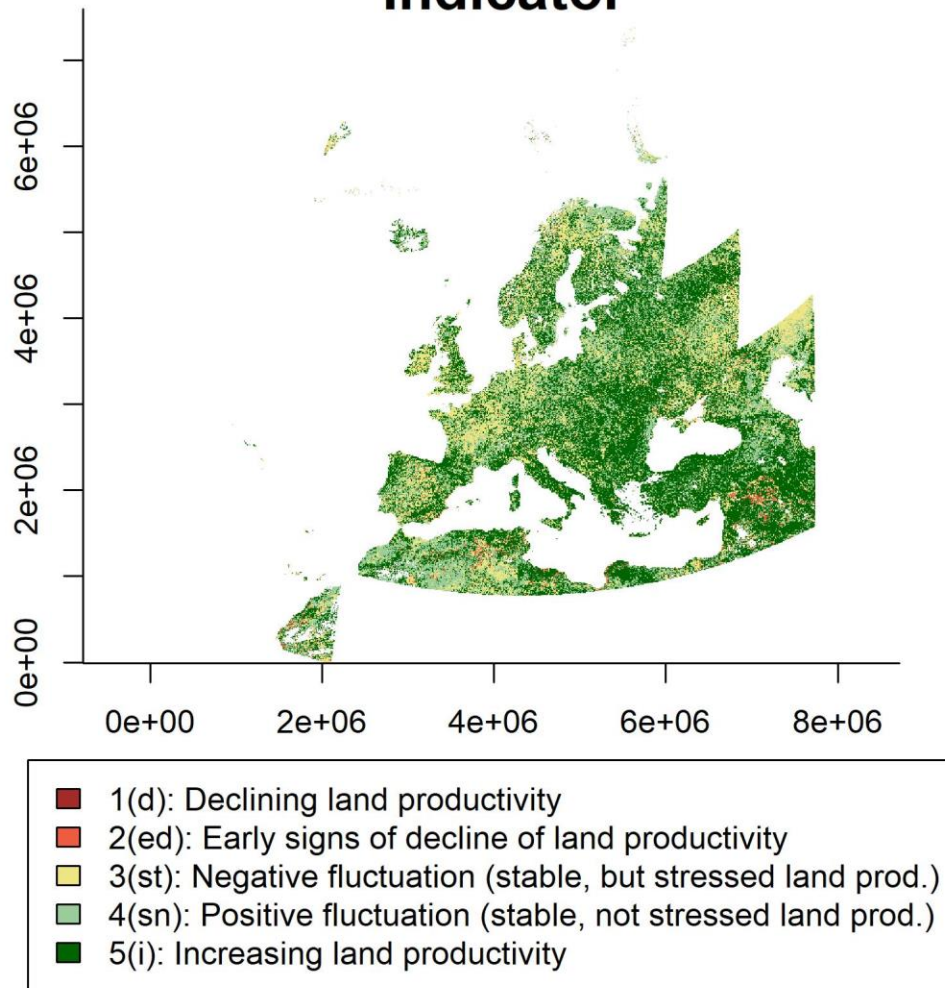
Steadiness I.	Baseline L.	State Change	Local Scaling	
			< 50%	>= 50%
st1	lo	0	d	ed
st1	lo	1	d	ed
st1	lo	2	d	d
st1	me	0	d	ed
st1	me	1	d	ed
st1	me	2	d	d
st1	hi	0	ed	st
st1	hi	1	d	ed
st1	hi	2	d	ed
st2	lo	0	st	st
st2	me	0	st	st
st2	hi	0	st	st
st3	lo	0	sn	sn
st3	me	0	sn	sn
st3	hi	0	sn	sn
st4	lo	0	sn	i
st4	lo	1	sn	i
st4	lo	2	i	i
st4	me	0	sn	i
st4	me	1	i	i
st4	me	2	i	i
st4	hi	0	i	i

447

448 In the present study, the Land Productivity Dynamics indicator final map (Figure 4) is the
 449 result of the combined assessment of the Long Term Change Map (Figure 2D) and the
 450 Current Status Map of land productivity (Figure 3B), both based on the “Above ground

451 vegetation productivity” variable, plus the two phenological variables for the derivation
452 of the EFTs.
453

Land Productivity Dynamics Indicator



454

455 *Figure 4: Land Productivity Dynamics indicator final map. Combined assessment of the Long*
456 *Term Change Map and the Current Status Map of land productivity.(1) d - Declining land*
457 *productivity, (2) ed - Early signs of decline of land productivity, (3) st - Stable but stressed land*
458 *productivity, (4) sn - Stable and not stressed land productivity and (5) i - Increasing land*
459 *productivity*

460 **6.1 Alternative method for the Land Productivity Dynamics indicator**

461 Including the current level of land productivity relative to its potential (Chapter 5) in the
462 final LPD calculation (Chapter 6) improves the land productivity indicator as LNS values
463 may indicate not degradation in areas with a negative tendency of productivity, but where
464 the level of productivity still remains high relative to other similar areas nearby. Despite
465 this, the user might want to derive the final product based only on the tendency map (i.e.
466 Long Term Change Map; Chapter 4), avoiding the inclusion of the Current Status Map
467 derived with the Local Net Scaling approach. The function *LPD_CombAssess()* performs
468 this step by passing the argument *LandProd_current = NULL*. By doing so, the function
469 reclassifies the Long Term Change Map into the same 5 categories of the LPD indicator
470 described above. Table 4 shows how the function executes the reclassification.

471

472

473

474

475

476

477

478

479 *Table 4: Lookup table for the reclassification of the Long Term Change Map into the Land*
 480 *Productivity Dynamics categories (i.e. (1) d - Declining land productivity, (2) ed - Early signs of*
 481 *decline of land productivity, (3) st - Stable but stressed land productivity, (4) sn - Stable and not*
 482 *stressed land productivity and (5) i - Increasing land productivity)*

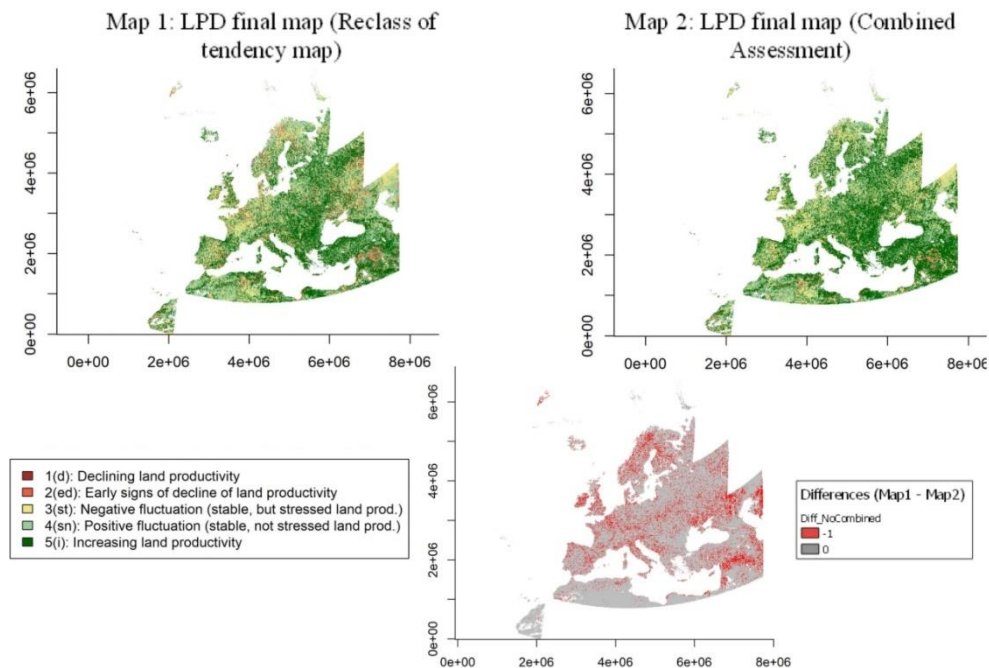
Steadiness I.	Baseline L.	State Change	LPD class
st1	lo	0	d
st1	lo	1	d
st1	lo	2	d
st1	me	0	d
st1	me	1	d
st1	me	2	d
st1	hi	0	ed
st1	hi	1	d
st1	hi	2	d
st2	lo	0	st
st2	me	0	st
st2	hi	0	st
st3	lo	0	sn
st3	me	0	sn
st3	hi	0	sn
st4	lo	0	sn
st4	lo	1	sn
st4	lo	2	i
st4	me	0	sn
st4	me	1	i
st4	me	2	i
st4	hi	0	i

483

484 A comparison of the final LPD indicator map produced using the combined assessment
 485 (i.e. Long Term Change Map + Current Status Map) with the one developed without the
 486 Current Status Map can be seen in Figure 5 (Map 1 and Map 2, respectively). In addition,
 487 the “differences map” in the same figure represents pixels which have a different class
 488 between the two approaches. The difference between the classes was always equal to

489 minus 1, indicating that the difference between the two approaches is only one class.
490 Furthermore, the combined indicator using the LNS approach had higher values in all
491 cases indicating a better potential to differentiate between land productivity conditions.
492 Table 5 shows the number of pixels which changed from one class to another. From this
493 table it can be seen how pixels never changed from negative to positive dynamics (class 3
494 to 4) or from positive to negative (class 4 to 3).

Comparison LPD final maps produced with Combined Assessment and with reclassification of Long Term Change Map



495

496 *Figure 5: Land Productivity Dynamics indicator final maps derived by the reclassification of the*
497 *Long Term Change Map of land productivity (Map 1) and produced by the combined assessment*
498 *(Map 2; Long Term Change Map + Current Status Map). Differences Map (Map 1 - Map2)*
499 *represents in red those pixels showing different resulting classes from both approaches*

500

501 *Table 5: Number of pixels showing different class in the combined assessment approach and in*
502 *the non-combined one (i.e. reclassification of the Long Term Change Map). Only these three*
503 *combinations were found in the case study*

Non-combined Assessment - Class	Combined Assessment - Class	Number Pixels	Description
1	2	2439370	Declining to early signs of decline
2	3	355412	Early signs of decline to Stable but stressed
4	5	4964183	Stable not stressed to Increasing

504

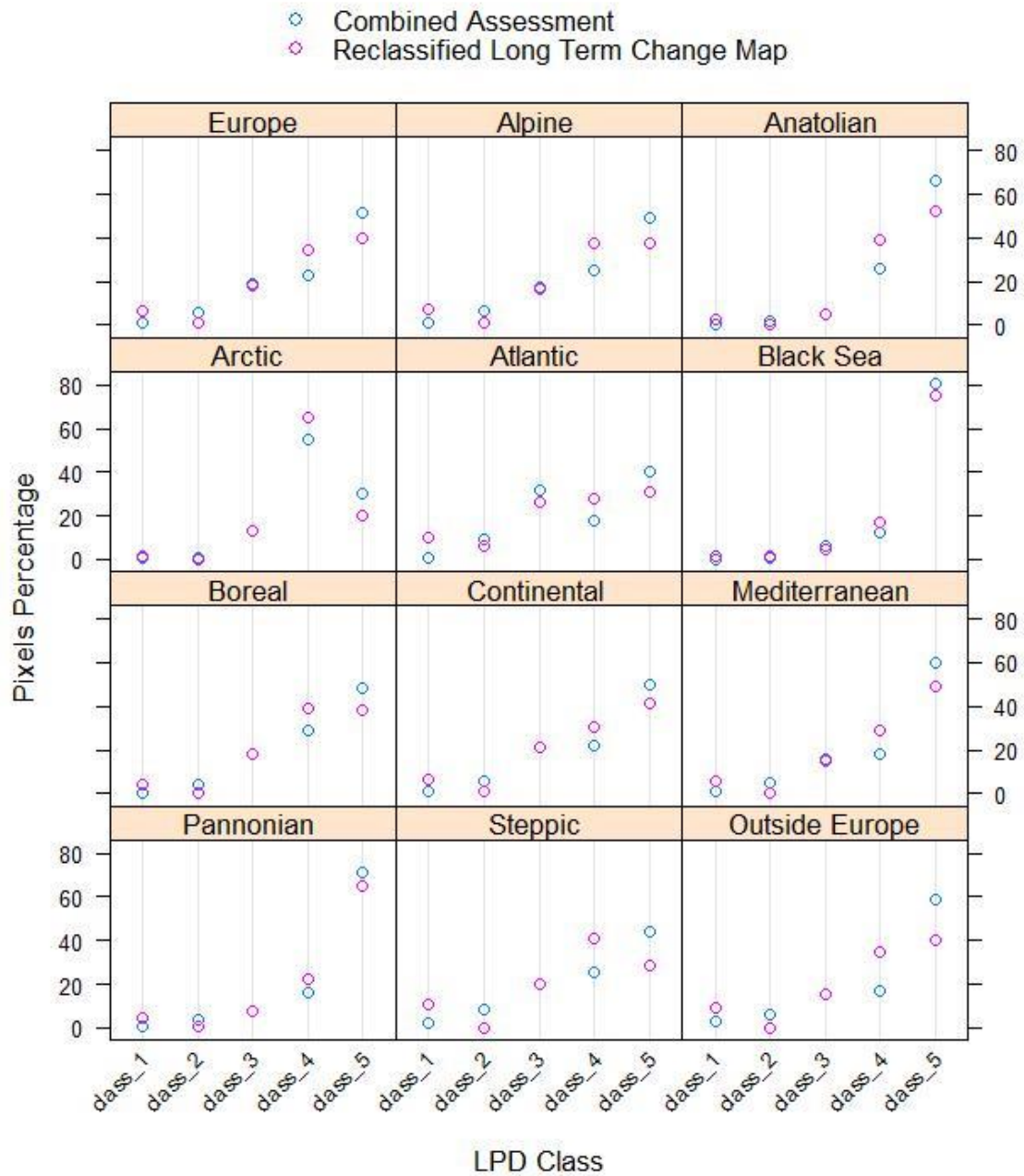
505 Finally, Figure 6 shows the proportion of pixels per LPD class under each approach, both
506 for the whole extent (i.e. Europe) and also splitting the map by biogeographical regions.

507 The biogeographical regions were defined with the official delineations used in the
508 Habitats Directive (92/43/EEC) and for the EMERALD Network, which are freely
509 distributed as a spatial data set by the European Environmental Agency - European
510 Commission ([https://www.eea.europa.eu/data-and-maps/figures/biogeographical-and-](https://www.eea.europa.eu/data-and-maps/figures/biogeographical-and-marine-regions-in)
511 [marine-regions-in](https://www.eea.europa.eu/data-and-maps/figures/biogeographical-and-marine-regions-in)).

512 The plots show that there were some differences in the proportion of pixels per class for
513 each of the two approaches. For example, the Alpine, the Anatolian, and the Steppic
514 regions were the three showing more differences, which ranged from 12.1 to 15.5% for
515 some LPD classes. This fact evidences the added value of including the Current Status
516 Map in the calculations to refine the LPD indicator final results.

517

Comparison LPD Methods by Bio-Geographical Regions (Combined Assessment vs Long Term Change M Reclassification)



518

519 *Figure 6: Proportion of pixels per LPD class for the combined assessment (light blue) and for the*
 520 *reclassified Long Term Change Map (purple), for Europe and by biogeographical regions*

521

522 **6.2 Land Productivity Dynamics partial indicator**

523 As seen in the previous subsections regarding the derivation of the tendency map (i.e.
524 Long Term Change Map; Chapter 4), the final result is related to the extremes of the time
525 series. In case the time series is long, the LPD indicator shows a long term assessment of
526 what has happened regarding the land productivity dynamics between the beginning and
527 the end of the period in the study. However, to understand the dynamics of the biomass
528 within the observation period, as well as to assess the stability of the final product, it
529 might be useful to produce several “partial LPD indicators” using different time windows
530 of the time series.

531 This process is not yet implemented in *LPD_{dynR}* as a function, but we propose the
532 following code to produce partial LPD maps of n years and with an overlap of y years
533 between the end of the last period and the beginning of the next one. This example was
534 implemented for the same case study shown along this article and the final partial LPD
535 maps can be seen in Figure 7.

536

537

538

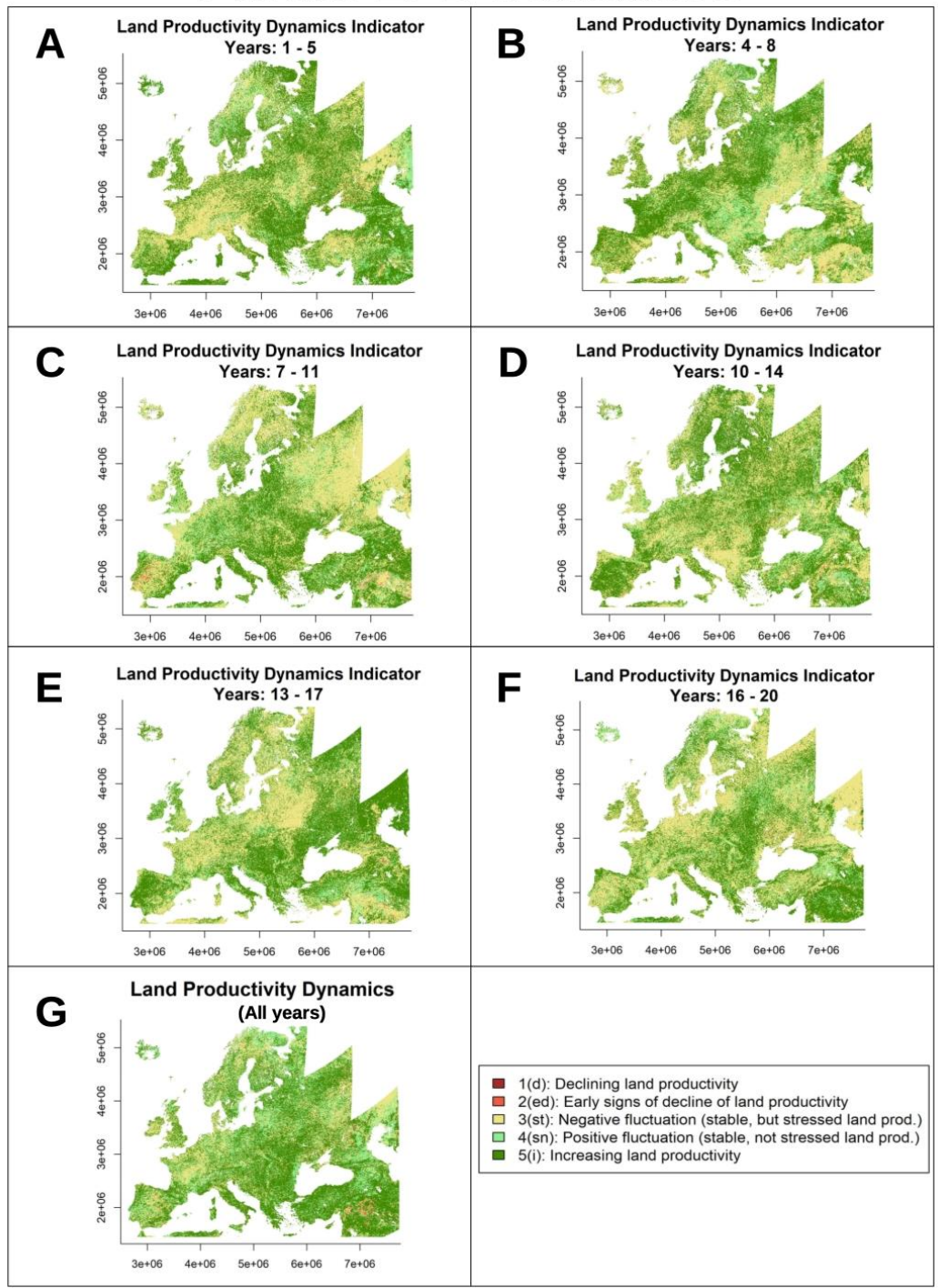
539

540

541

```
542 ## Running LPDynR for partial time series ##
543
544 ts_length<- 5 # time series length to run 'partial LPD maps'
545 ts_years_overlap <- 2 # number of years of overlapping
546 partial_dir<- "/LPD_partial" # directory to save the 'partial LPD' results
547 first_year<- 1 # first year of the whole time series
548 last_year <- nlayers(cf) # last year of the whole time series
549 last_year_run<- first_year + ts_length - 1 # last year of the 'partial LPD'
550
551 while(last_year_run <= last_year){
552 # subsetting the years (layers) to run
553 cf_run <- cf[[first_year:last_year_run]]
554
555 # a directory to save the data
556 dir2save0<- paste0(getwd(),partial_dir)
557 if(!dir.exists(dir2save0)) dir.create(dir2save0)
558 dir2save <- paste0(getwd(),partial_dir,"/LPD_",first_year,"_",last_year_run,"/")
559 if(!dir.exists(dir2save)) dir.create(dir2save)
560
561 ## ##
562 ## ##
563 ## Here all the steps to calculate the ##
564 ## final LPD map as in the examples ##
565 ## ##
566 ## ##
567
568 # Cleaning temp
569 removeTmpFiles(h = 0.5)
570
571 # Parameters for the loop
572 first_year<- last_year_run - ts_years_overlap + 1
573 last_year_run <- first_year + ts_length - 1
574 }
575
```


Partial LPD Indicators



576

577 Figure 7: Partial LPD indicators (plots A to F) and LPD indicator for the whole time series (plot
578 G). The partial LPD indicators were produced for time windows of 5 years with an overlap of 2
579 year between the end of the last period and the beginning of the next one

580 The complete LPD indicator (i.e. for the whole time series; Figure 7G) shows, in general
581 terms, a positive trend pattern across Europe (i.e. more pixels in greens). However, some
582 of the intermediate plots show more negative trends (i.e. yellow and light red pixels).
583 This, besides demonstrating the highly fluctuating character of vegetation, confirms the
584 influence of the extremes of the time series on the final result. In this sense, in the time
585 series of the example, the first period seemed to show stressed vegetation in terms of
586 productivity for most of the pixels in Western/Central Europe, and they expressed a large
587 increase around years 7/8. Such increase caused a large number of areas belonging to the
588 higher LPD class, and it still influenced the dynamics of the following period, resulting in
589 areas with stressed vegetation.

590 The fact that the LPD indicator calculated with the approach included in *LPD_{dynR}* is
591 influenced by the beginning and the end of the time series is not a limitation, as the main
592 goal of the LPD indicator is to know the current state of vegetation in relation to a
593 previous state, and not the fluctuations due to, for example, to extreme climatic events
594 such as e.g. droughts. However, being able to map these fluctuations in space and time
595 might add information for further analysis.

596 **7 Conclusions**

597 As stated by the Intergovernmental Science-Policy Platform on Biodiversity and
598 Ecosystem Services (IPBES), land degradation leads to a loss of biodiversity and a
599 reduction of ecosystem functions and delivered services all over the world. Therefore,
600 combating land degradation and restoring degraded lands has become an urgent priority
601 in order to protect all life on Earth as well as to ensure human well-being (IPBES, 2018).

602 In this sense, satellite observations provide valuable data which might help to monitor the
603 Earth's land cover to evaluate the state of land degradation.

604 The Land Productivity Dynamics indicator (LPD), as part of the SDG-15.3.1 indicator,
605 aims at contributing to the assessment of the state of land degradation and desertification
606 at global, regional and local scales. Therefore, the *LPD_{dynR}* new tool has been developed
607 to derive the LPD indicator using phenological and land productivity variables, which
608 can be obtained from long-term time series of Earth observation imagery.

609 *LPD_{dynR}* is a comprehensive set of open source programming code, written in the well-
610 known R language and properly packaged, ready to be freely distributed in order to let
611 the users with a minimum knowledge of the R language calculate the LPD indicator. The
612 package, once installed, includes several examples and a small data set for testing the
613 functionalities and the different parameters to tune them.

614

615

616 **8 References**

617 Cherlet, M., Hutchinson, C., Reynolds, J., Hill, J., Sommer, S., Maltitz, G. von (Eds.),
618 2018. World atlas of desertification. Publication Office of the European Union,
619 Luxembourg.

- 620 Dubovyk, O., 2017. The role of remote sensing in land degradation assessments:
621 Opportunities and challenges. *European Journal of Remote Sensing* 50, 601–613.
622 <https://doi.org/10.1080/22797254.2017.1378926>
- 623 FAO, 2019. Trees, forests and land use in drylands: The first global assessment (FAO
624 Forestry Paper No. 184). FAO, Rome.
- 625 Fensholt, K.K., Rasmus Rasmussen, 2013. Assessing land degradation/recovery in the
626 african sahel from long-term earth observation based primary productivity and
627 precipitation relationships. *REMOTE SENSING* 5, 664–686.
- 628 Guo, W.Q., Yang, T.B., Dai, J.G., Shi, L., Lu, Z.Y., 2008. Vegetation cover changes and
629 their relationship to climate variation in the source region of the yellow river, china,
630 1990–2000. *International Journal of Remote Sensing* 29, 2085–2103.
631 <https://doi.org/10.1080/01431160701395229>
- 632 IPBES, 2018. The ipbes assessment report on land degradation and restoration.
633 Montanarella, l., scholes, r., and brainich, a. (Eds.). Secretariat of the
634 Intergovernmental Science-Policy Platform on Biodiversity; Ecosystem Services,
635 Bonn, Germany.
- 636 Ivits, E., Cherlet, M., 2013. Land-productivity dynamics towards integrated assessment
637 of land degradation at global scales (Technical Report No. EUR 26052). Joint
638 Research Centre of the European Commission.
- 639 Ivits, E., Cherlet, M., Horion, S., Fensholt, R., 2013. Global biogeographical pattern of
640 ecosystem functional types derived from earth observation data. *Remote Sensing* 5,
641 3305–3330. <https://doi.org/10.3390/rs5073305>

- 642 Ivits, E., Cherlet, M., Mehl, W., Sommer, S., 2013. Ecosystem functional units
643 characterized by satellite observed phenology and productivity gradients: A case
644 study for europe. *Ecological Indicators* 27, 17–28.
645 <https://doi.org/10.1016/j.ecolind.2012.11.010>
- 646 Ivits, E., Cherlet, M., Sommer, S., Mehl, W., 2013. Addressing the complexity in non-
647 linear evolution of vegetation phenological change with time-series of remote
648 sensing images. *Ecological Indicators* 26, 49–60.
649 <https://doi.org/https://doi.org/10.1016/j.ecolind.2012.10.012>
- 650 Jin, H., Eklundh, L., 2014. A physically based vegetation index for improved monitoring
651 of plant phenology. *Remote Sensing of Environment* 152, 512–525.
652 <https://doi.org/https://doi.org/10.1016/j.rse.2014.07.010>
- 653 Jönsson, P., Eklundh, L., 2004. TIMESAT—a program for analyzing time-series of
654 satellite sensor data. *Computers & Geosciences* 30, 833–845.
- 655 Leroy B., Meynard C.N., Bellard C., Courchamp F., 2016. virtualspecies, an R package
656 to generate virtual species distributions. *Ecography* 39, 599-607.
657 <https://doi.org/10.1111/ecog.01388>
- 658 Middleton, N., Stringer, L., Goudie, A., Thomas, D., 2011. The forgotten billion. MDG
659 achievement in the drylands. United Nations Development Programme, New York,
660 NY, 10017, USA.
- 661 Orr, B.J., Cowie, A.L., Castillo Sanchez, V.M., Chasek, P., Crossman, N.D., Erlewein,
662 A., Louwagie, G., Maron, M., Metternicht, G.I., Minelli, S., Tengberg, W., A. E.,

- 663 Welton, S., 2017. Scientific conceptual framework for land degradation neutrality.
664 In: A report of the science-policy interface. UNCCD, Bonn, Germany.
- 665 Prince, I.R., S. D. Becker-Reshef, 2009. Detection and mapping of long-term land
666 degradation using local net production scaling: Application to zimbabwe.
667 REMOTE SENSING OF ENVIRONMENT 113, 1046–1057.
- 668 Sims, N.C., Barger, N.N., Metternicht, G.I., England, J.R., 2020. A land degradation
669 interpretation matrix for reporting on un sdg indicator 15.3.1 and land degradation
670 neutrality. Environmental Science & Policy 114, 1–6.
671 <https://doi.org/https://doi.org/10.1016/j.envsci.2020.07.015>
- 672 Sims, N.C., Green, C., Newnham, G.J., England, J.R., Held, A., Wulder, M.A., al., 2017.
673 Good practice guidance sdg indicator 15.3.1. Proportion of land that is degraded
674 over total land area, First. ed. United Nations Convention to Combat
675 Desertification.
- 676 UN, 2015. Transforming our world: The 2030 agenda for sustainable development (No.
677 A/RES/70/1). United Nations.
- 678 UNCCD, 2015. Integration of the sustainable development goals and targets into the
679 implementation of the United Nations convention to combat desertification and the
680 report of the intergovernmental working group on land degradation neutrality (No.
681 ICCD/COP(12)/4). UNCCD Conference of the Parties, Ankara, Turkey.
- 682 Yengoh, G.T., Dent, D., Olsson, L., Tengberg, A.E., Tucker, C.J., 2015. Use of the
683 normalized difference vegetation index (ndvi) to assess land degradation at multiple
684 scales, Springer briefs in environmental science. Springer.